



Research Article

An effective method for paleo-temperature correction of 3D thermal models: A demonstration based on high resolution datasets in the Netherlands



Casper Gies ^{a,*}, Maartje Struijk ^b, Eszter Békési ^a, Hans Veldkamp ^b, Jan-Diederik van Wees ^{a,b}

^a Department of Earth Sciences, Utrecht University, Utrecht 3584, CB, Netherlands

^b TNO Utrecht, Utrecht 3584, CB, Netherlands

A B S T R A C T

We present a new method to incorporate paleo-surface temperature effects in steady state 3D conductive temperature models. The workflow approximates the transient effects and incorporates these into steady state models, using appropriate source and sink terms for radiogenic heat production. This allows for rapid models, which can be easily used in ensemble approaches for data assimilation of high-resolution temperature models for geothermal resource assessment. The workflow is demonstrated for the Netherlands which is a sedimentary basin with a wealth of deep (temperature) data from groundwater and oil and gas wells and past studies on the 3D temperature distribution. 3D subsurface temperature models of the Netherlands ranging up to 5 km depth systematically overpredict temperatures at shallow (<1500 m) depth. Analysis of both shallow (<600 m, >200,000 measurements) and deep temperature measurements (1–6 km, >1500 measurements), clearly demonstrates a shallow thermal gradient in over 200 locations of $\sim 20 \text{ }^{\circ}\text{C km}^{-1}$ for the top 400 m underlain with a deep geothermal gradient of $\sim 31 \text{ }^{\circ}\text{C km}^{-1}$ for the 2–4 km interval. Improvements in 3D subsurface modelling regarding the shallow part are accomplished by adding a paleo-surface temperature correction related to glaciation effects of the Weichselian glacial period. This paleo-surface temperature correction proved to be the missing link between two distinctive geothermal gradients observed and is consistent with earlier findings for limited datasets. The consistent overprediction of modelled temperatures in 74% of locations for the top 2 km which are regularly distributed over the Netherlands demonstrates that the influence of paleo-surface temperatures is rather uniform over large areas and not significantly overprinted by other effects such as groundwater flow. The updated model, marked by up to 10 degrees cooling compared to models ignoring the paleo-surface temperature effects, has major implications for assessing geothermal resource potential up to 2 km depth.

1. Introduction

Geothermal energy is a renewable energy source that is sustainable for future generations and available autonomous of seasonal fluctuations or changing climate conditions. Geothermal energy can be used as direct heat source or to generate electricity. Geothermal energy is therefore very well suited to incorporate in the transition from a fossil-based energy system to a renewable and sustainable energy regime. To define the geothermal potential, the temperature distribution is one of the most important parameters to investigate (e.g. Beardmore et al., 2010). On continental scale -outside magmatic areas marked by strong transient effects- mostly 1D thermal conductive models have been used for resource assessment (e.g. Limberger et al., 2014; Limberger et al., 2018), whereas on more regional (national) scale, in various countries high resolution 3D thermal models have been constructed constrained by temperature data from deep boreholes (e.g. Bonté et al., 2012; Gola et al., 2017; Békési et al., 2020). 3D steady state conductive models are very effective in terms of computational performance for high resolution

models (e.g. Békési et al., 2020).

The application of steady state models has limitations which need to be carefully considered for settings or depth ranges where transient effects are present. For example, in regions marked by relatively rapid sediment and erosion and active tectonism, temperature distributions can be strongly affected (e.g. Van Wees et al., 2009; Cloetingh et al., 2010; Limberger et al., 2018). Hydrothermal fluid flow and associated heat advection-mostly observed more locally- can also give rise to strong alteration of the steady state predictions, even at a few km depth (e.g. Majorowicz and Wybraniec, 2011; Lipsey et al., 2016). In addition, paleo-surface temperature changes, in particular the effects of past glaciations can strongly affect the observed surface heat flow values and temperature gradient in the top few km of the earth and give rise to relative low geothermal gradient in the top 1–2 km of the crust and sediments relative to the deeper part, which is well recorded in boreholes (e.g. Ter Voorde et al., 2014).

For geothermal exploration, the relative shallow sedimentary layers up to 2 km depth are generally prospective for geothermal energy

* Corresponding author.

E-mail address: casper_gies@hotmail.com (C. Gies).

production in view of relatively good flow properties, due to limited compaction of pores (e.g. Van Wees et al., 2012). In addition, the shallow layers can be used for High Temperature Aquifer Thermal Energy Storage (HT-ATES) (Wesselink et al., 2018). For these reasons, it is of importance for the shallow depth range to take into account the paleo surface temperature effects to accurately predict the temperature distribution for performance assessment.

In this paper, we present an effective 3D workflow for correcting steady state thermal models for paleo surface temperature evolution. We apply the workflow in constructing high resolution temperature models. We have chosen to develop and demonstrate the approach to the Netherlands for the following reasons: the availability of both shallow and deep temperature data, high resolution structural models, previous thermal models and paleo surface temperature scenarios models.

The first 3D temperature model of the Netherlands has been constructed by Bonté et al. (2012), which is based on a purely conductive methodology including transient effects of vertical motion and surface temperature over the basin history, calibrated with temperature data from oil, gas and geothermal wells. This model could not explain the temperature anomalies at larger depth (e.g. >3 km). Taking into account new geological insights at larger depth like the buried Dinantian carbonate platforms (within the Limburg Group), adding newly available temperature data and a pseudo-convection approach (cf. Lipsey et al., 2016), using an improved data-assimilation technique, the 3D temperature model has been recently updated by Békési et al. (2020) and is available at ThermoGIS (<https://www.thermogis.nl/>).

Models and temperature measurements from oil, gas and geothermal wells at depths between 2 and 4 km show an almost linear geothermal gradient of about $31^{\circ}\text{C km}^{-1}$; with T is temperature ($^{\circ}\text{C}$) and z is depth (km) (Bonté et al., 2012):

$$T(z) = 10 + 31.3z \quad (1)$$

Békési et al. (2020) found a tendency in the model to overestimate temperatures compared to observations at the shallow part of the model (<2 km) (Fig. 4). Therefore, they tried to correct the model by assuming a surface temperature of 8°C while it is known to be $\sim 10^{\circ}\text{C}$ (Békési et al., 2020). The consistent positive misfit of previous models for the top 2 km could possibly be explained by the cooling effect of paleo-surface temperatures which has been demonstrated by Ter Voorde et al. (2014) in 1D models (Pollack and Huang, 2000; Bodri and Cermak, 2011; Huang et al., 2008; Majorowicz and Šafanda, 2008; Kukkonen et al., 2011; Majorowicz and Wybraniec, 2011). Alternatively, the influence of groundwater flow at shallow depth could explain anomalies observed (Smith and Chapman, 1983; Kooi, 2016; Bense et al., 2020). Earlier research about the thermal field of the Dutch subsurface from Van Dalsen (1980a) showed an average geothermal gradient of $\sim 20^{\circ}\text{C km}^{-1}$ for the top ~ 400 m.

The aim of this study is to make a connection between two distinctive geothermal gradients previously observed, one steeper deep ($\sim 31^{\circ}\text{C km}^{-1}$) (Bonté et al., 2012; Békési et al., 2020) and one flatter shallow ($\sim 20^{\circ}\text{C km}^{-1}$) (Van Dalsen, 1980a). To this end, in this research, more data are added to the database as input to thermal models for the Netherlands, using temperature measurements of 471 boreholes from the shallow subsurface between 0 and 500 m. In addition, modifying the existing steady state workflow (Békési et al., 2020), we present an extended workflow to include the transient effects of paleo surface temperature changes for the 3D model capable of explaining the two different geothermal gradients. The updated 3D subsurface temperature model including the extra temperature data and transient thermal effects of paleo-surface temperature changes are of major importance to better understand the shallow thermal regime, and can have considerable implications for estimating the potential for shallow geothermal energy and High Temperature Aquifer Thermal Energy Storage (HT-ATES) facilities of the onshore Netherlands.

2. Geological setting

The basis for 3D temperature modelling of the Dutch subsurface is the regional-scale 2.5D geologic framework, the Digital Geological Model (DGM-deep v4.0) (Fig. 1). The first version of the geological model used has been constructed in 1985 to support the hydrocarbon E&P industry (Kombrink et al., 2012). Although this model was constructed for the hydrocarbon industry, increased interest in geothermal energy and heat storage, like the SCAN project (Seismic Campaign Geothermal Netherlands) (e.g. Carlson, 2019) now mainly drives improvements of the geological model.

DGM-deep v4.0 is built upon 14 separate geologic formations which are described in more detail at www.dinoloket.nl/en/nomenclature-deep (Van Adrichem Boogaert and Kouwe, 1993). These 14 geologic formations are based upon the geologic history of the Netherlands starting at the Carboniferous. During the Carboniferous the Netherlands was situated in the northern foreland of the Variscan Orogeny. In the Early Carboniferous in the north carbonate platforms developed while in the south late Carboniferous Silesian sandstones, coals and shales from the southern Variscan thrusts were deposited (Kombrink et al., 2010; Van Hulten and Poty, 2008). The Late Carboniferous was characterised by the orogenic collapse of the Variscan orogeny with a major hiatus between the Carboniferous and Permian rocks with locally observed magmatic intrusions (Sissingh, 2004; Van Wees et al., 2000; Smit et al., 2018). The post-Variscan basin accumulated space for deposition of Rotliegend and Zechstein sediments (Van Wees et al., 2000; Kombrink et al., 2010). In the northern Netherlands mostly marine evaporites were deposited while the southern Netherlands was marked by deposition of more siliciclastic and carbonate-like rocks. The gradual break-up of Pangea during Triassic times resulted in deposition of clastic sediments alternated with minor shale deposits. The Altena Group represents the transition from shallow marine deltaic sedimentation to fully marine deposition of argillaceous sediments (Kombrink et al., 2012). A rifting phase created accumulation space to deposit Late Jurassic and Early Cretaceous shallow marine siliciclastic sediments of the Rijnland and Schieland Group with subsequently Cretaceous Chalk (Kombrink et al., 2012). Compressional stresses during the Late Cretaceous led to the first inversion phases with siliciclastic depositions in the Early Paleogene (De Jager, 2003). Later inversion led mostly to erosion and subsequent rifting phases during the Cenozoic caused Paleogene sedimentation characterised by an alternation of sand and clay. The remaining accommodation space is continuously filled by the development of a delta system at Neogene time (Kombrink et al., 2012).

3. Temperature data

In previous versions of the model, temperature measurements from oil, gas and geothermal wells including Bottom Hole Temperatures (BHTs), Drill Stem Test (DST) temperatures and Repeat Formation Tests (RFT) have been used for calibrating the model (Békési et al., 2020). This database (from now called: "Deep database") is freely available (<http://www.nlog.nl/>) (<http://www.geothermie.nl>) and provides over 1507 temperature measurements from a 1 to 6 km depth range. This "Deep database" however lacks accurate shallow temperature measurements and is expanded in this study with an additional shallow temperature database.

The additional shallow temperature database (from now called: "Shallow database") originates from the Dutch groundwater survey of TNO (<https://www.dinoloket.nl/>). The "Shallow database" contains all groundwater boreholes to a maximum depth of ~ 500 m that are commissioned by TNO. Data from the "Shallow database" predominantly originates from studies of the groundwater survey TNO in the period 1975–1983 (Van Dalsen, 1980a; Van Dalsen, 1983b). This data is commissioned by the geothermal energy program from The Commission of the European Communities to obtain temperatures at 250 m depth of the Dutch subsurface and coexisting heat flow densities. A total

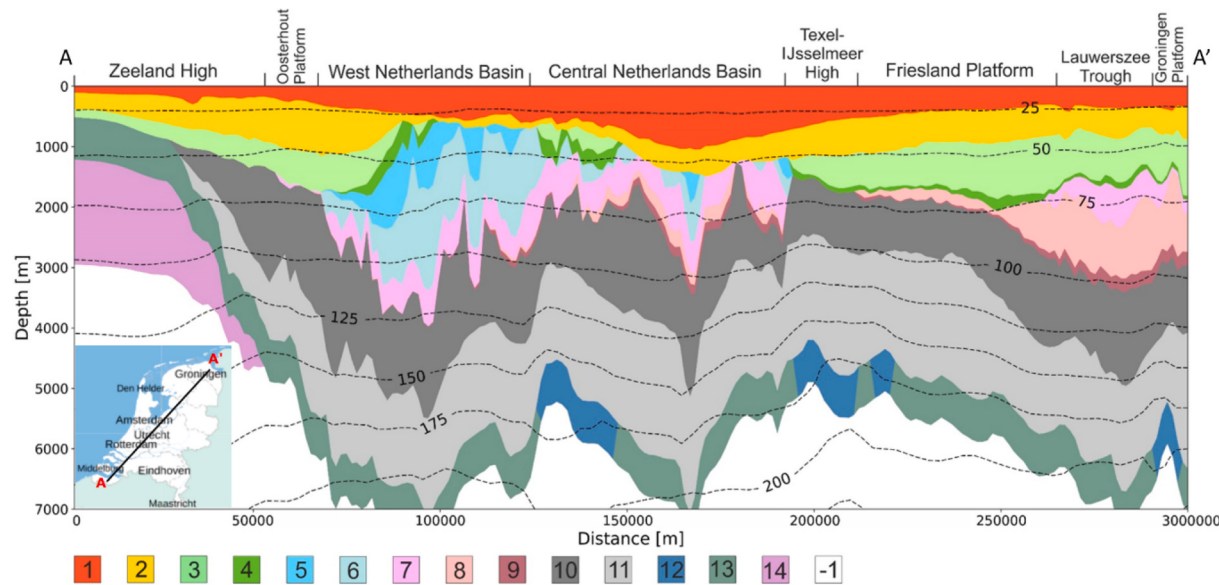


Fig. 1. “NW-SE cross-section through the onshore Netherlands showing the geometry of the sedimentary units and the depth of the top of the basement (white) used for modelling. Superimposed are the isotherms from the temperature model” from Békési et al. (2020). Sedimentary units correspond to DGM-deep v4.0 (Kombrink et al., 2012) (e.g. 1: Upper North Sea Group (NU), 2: Lower/Middle North Sea Group (NL, NM), 3: Chalk Group (CK), 4: Rijnland Group (KN), 5: Schieland Group (S), 6: Altena Group (AT), 7: Lower and Upper Germanic Trias Group (RB, RN), 8: Zechstein Group (ZE), 9: Rotliegend Group (RO), 10: Limburg Group (DCC, DCD, DCH), 11: Limburg Group (DCG), 12 & 13: Carboniferous Limestone Group (CL, CF), 14: Old Red Group and Banjaard Group (OR, OB) & -1: Bedrock).

of 471 wells include 223,426 distinct temperature measurements. Approximately every meter the temperature has been measured and recorded over the whole drilling interval. The temperature measurements within the “Shallow database” originate mainly (97.5%) from a depth down to 400 m. No more than 12 wells exceed a depth of 400 m with two (0.4%) wells reaching down to 1500 m. Fig. 2 and b show in more detail the depth of the temperature measurements from the “Deep database” (red) and “Shallow database” (blue) while Fig. 2c shows a spatially good coverage of the “Combined database” for the whole onshore Netherlands.

3.1. Data quality

A key difference between the “Shallow database” and “Deep database” is the amount, regularity, and quality of the temperature measurements. Temperature measurements of the “Deep database” vary in depth between 200 m and 6000 m, with 85% of the data located in the domain between 1000 m and 4000 m, and up to 2 km depth hold measurement errors ranging from 5 °C to 15 °C (Bonté et al., 2012; Békési et al., 2020). Data obtained from the “Shallow database” is considered very reliable, with an error margin of 0.1–2.0 °C. This low error margin is obtained by using a small borehole diameter and the use of poorly heat-conducting materials (Van Dalsen, 1981b). The largest 2 °C error for the worst reliable data has been determined by the method of Mundry (Kappelmeyer and Haenel, 1974; Van Dalsen, 1980a; Van Dalsen, 1983b). Evidently, error margins of the “Deep database” are large compared to the “Shallow database”. As the “Shallow database” is marked by significantly lower errors than the “Deep database” and shows a good geographical coverage, we therefore ignore data from the deep database below 400 m in the remainder of the paper. Of the “Shallow Database”, only temperature measurements closest to every 200 m in depth are selected. This selection is fundamental since the model uses a vertical grid size of 200 m, which is further described in Section 4. The resulting merged database is used as input for the modelling and called the “Combined database”.

3.2. “Shallow Database” analysis and anomalies

Since this study uses data recorded over a timespan of four decades during all seasons, the moment of measuring can influence the temperature. It is known that seasonal fluctuations influence the subsurface to a depth of 15–20 m (Bense and Kooi, 2004), therefore temperatures shallower than 15 m have been excluded. Since the 1980s also average surface temperatures raised and affect the geotherm to depths of 70 m (Kooi, 2008). Months and years of drilling are listed to inspect if this affected the “Shallow database”. Monthly changes in subsurface temperature are clearly visible whereas yearly changes are not clearly visible within the “Shallow database”.

The “Shallow database” showed other phenomena that causes perturbations in the thermal structure in the very shallow subsurface, up to approximately 150 m depth. Studies like: Peters et al. (1983); Van Dalsen (1980b); Van Dalsen (1981a); Van Dalsen (1983a) and Van Dalsen (1998), list and explain these local anomalies at several wells of the “Shallow database”:

- Local effects of landfill or water exploitation are visible in the top part of the subsurface within the “Shallow database”. The dataset contains several wells specifically drilled to investigate thermal effects of water exploitation or landfill, explaining local anomalies like in Fig. 3a & b.
- The urban heat island effect represents a 2.0 °C higher average air and surface temperature in urban areas compared to surrounded countryside (Conrads, 1975; Unger, 1992). Buildings and traffic are responsible for temperature elevations at urban areas because heat is stored over a longer period at these objects. High buildings create a perpendicular reflectance of sunlight that increases the temperature faster at mornings when the sun comes up (Stolk, 2000). Consequently, subsurface temperatures of wells drilled in urban areas are elevated due to the extra heat abundant in cities. This effect would potentially be visible to a depth of 120 m (Zhu, 2013a). The top part of the geotherm of an affected well drilled in an urban area has a so-called inverse shape due to heating from the top (Fig. 3c), while unaffected wells have a linear geotherm, if no other local effect is influencing the well site (Buik et al., 2004; Stolk, 2000).

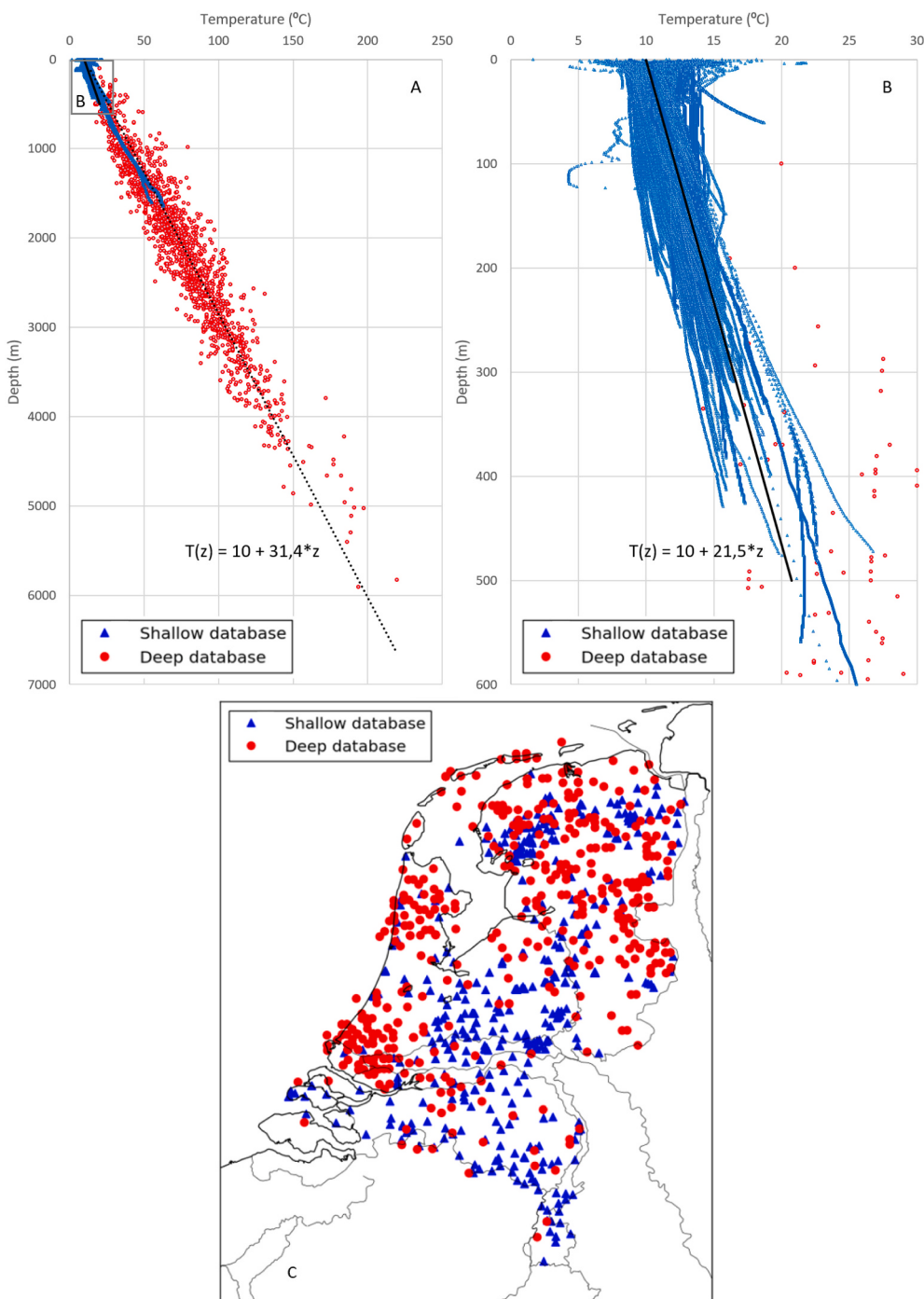


Fig. 2. a) and b). Temperature measurements of the “Combined database”, where the dotted black line and corresponding equation represent the average geotherm from the “Deep database” (Békési et al., 2020). The solid black line and corresponding equation represent the average geotherm of the “Shallow database” like Van Dalfsen (1980a). c). Well locations of the “Combined database”.

- A change in land use, from forest to agricultural or agricultural to urban over the last decades shows similar effects with affected geotherms (Kooi, 2008). This effect is only recognizable at the top 50 m of the geotherm.

Therefore, temperatures shallower than 100 m need to be interpreted with caution, and the data should not just be extrapolated as regional trend based on local changes in temperature.

3.3. Overestimation of temperature data by previous 3D models

For the “Combined database” we compared the misfit of the modelled temperatures of Békési et al. (2020) at intervals of 200 m, down to 2 km depth in Fig. 4. Positive mean and median values of the modelled versus observed temperatures indicate that models systematically overestimate temperature measurements for the whole depth range, for 74% of the “Combined database”. This overestimation of the model is consistent for both databases, with a 100% overestimation of the temperature measurement in the “Shallow database” exceeding 100 m depth and 71% of the measurements in the “Deep database”. Modelled

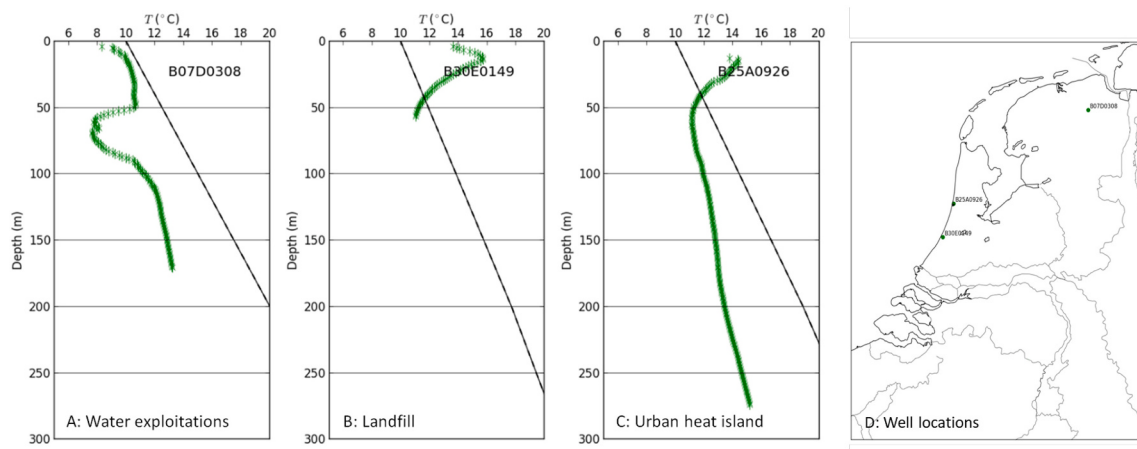


Fig. 3. Temperature/depth plots of local anomalies for three random locations within the “Shallow database” of the onshore Netherlands. Temperature observations (green) compared to modelled temperature (black) from Békési et al. (2020). (For interpretation of the references to colour in this figure legend, the reader is referred to the web version of this article.)

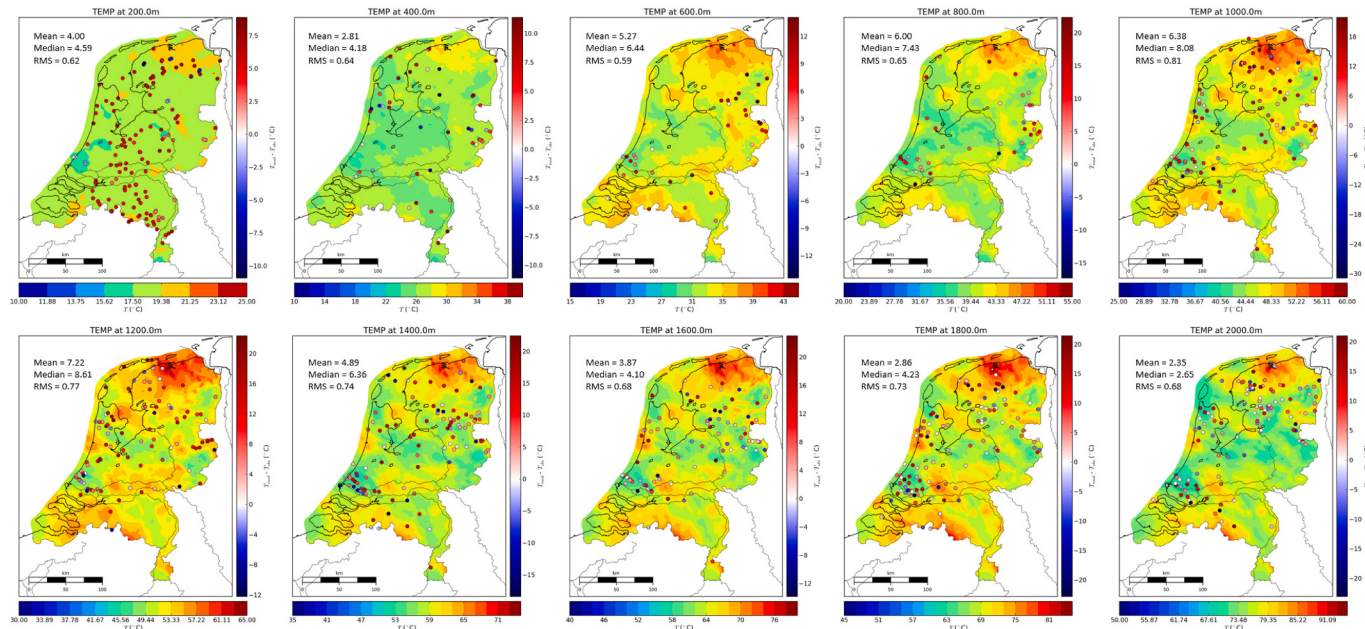


Fig. 4. Isodepth temperature maps of the onshore Netherlands between 200 and 2000 m depth of Békési et al. (2020). Modelled temperatures minus observed temperatures from the “Combined database” are plotted on top with circles within a ± 100 m interval. Note the different colour scale for modelled temperatures at various depth. “Mean”, “Median” and “Root Mean Square(RMS)” values refer to the difference between the modelled temperature and the data.

temperatures of Békési et al. (2020) in the depth range of 2–6 km show good fit with temperature observations from the “Deep database” with 53% under- and 47% overestimated temperatures. The average overestimation of the model is $\sim 4^{\circ}\text{C}$ at 200 m and increases towards $\sim 8^{\circ}\text{C}$ at 1000/1200 m depth. The biggest mismatch between modelled and observed temperatures is found within the depth interval of 200–1200 m. From 1 to 2 km depth the systematical average overestimation decreases again towards $\sim 2.5^{\circ}\text{C}$ at 2 km depth.

4. Methodology

The updated 3D subsurface temperature model follows the same workflow as Békési et al. (2020) used to compute the previous 3D subsurface temperature model, including identical grid sizes and thermal properties. We solved the inverse problem using the Ensemble Smoother (ES), which estimates the parameters in a single step by a global update incorporating all data available (Emerick and Reynolds, 2013). We

applied the Ensemble Smoother with multiple data assimilation (ES-MDA) for handling the non-linearity between the observations and model parameters (Békési et al., 2020). This workflow is however expanded with two intermediate steps between the high-resolution Prior 3D model (Step 6) and high-resolution Posterior 3D model (Step 7) Békési et al. (2020). In the modified workflow depicted in Fig. 5, in step 6 (now labelled step 6a–c) first the cooling effect of paleo-surface temperatures on subsurface temperatures is predicted (step 6b) in a transient forward model approach similar to Ter Voorde et al. (2014). The approach is explained in more detail in Section 4.1. Subsequently, this cooling effect on the subsurface temperature distribution is precisely transferred to the steady state model adopting a correction in radiogenic heat production in the top of the 3D thermal model (step 6c). These additional steps are added to the workflow just before a final run of extensive data assimilation, as performed by Békési et al. (2020).

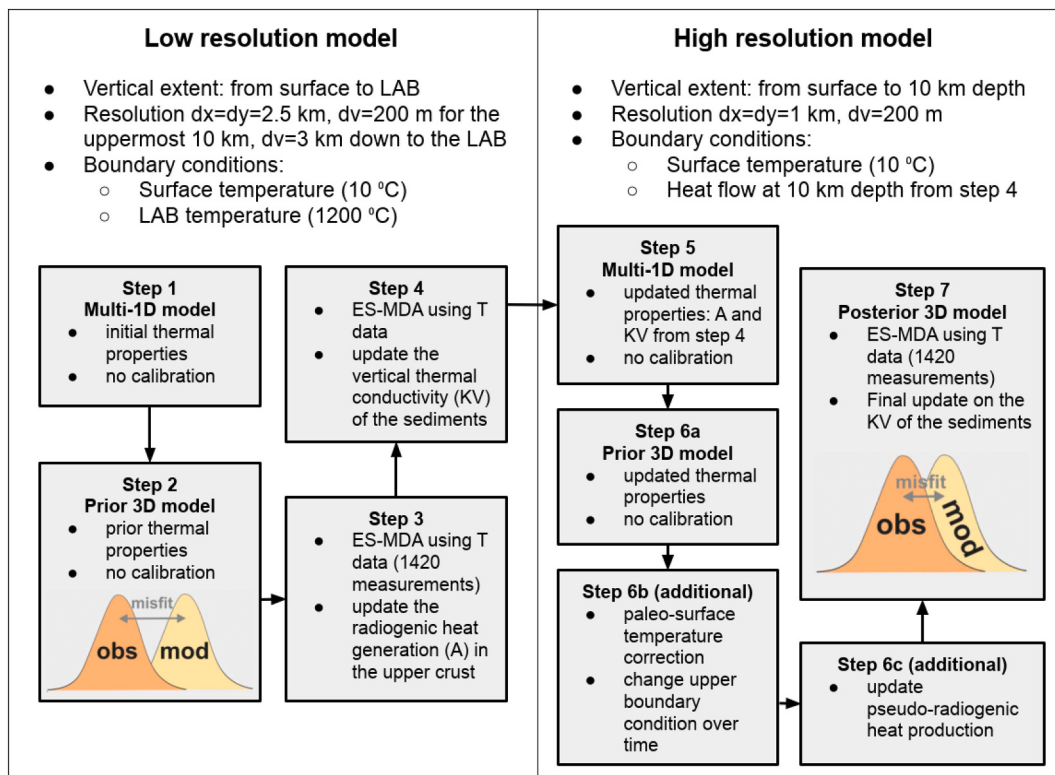


Fig. 5. Description of the modelling workflow after Békési et al. (2020). LAB: Lithosphere-Asthenosphere Boundary. ES-MDA: Ensemble Smoother with Multiple Data Assimilation.

4.1. Paleo-surface temperature history

To represent paleo-surface temperatures in the Netherlands over the last 130,000 years, the temperature evolution proposed by Luijendijk et al. (2011) is used (Fig. 6). The temperature evolution covering Eemian, Weichselian and Holocene times is based on climate proxy data like fossil beetles (Coleoptera), pollen, plant macro remains and periglacial indicators in northwest and central Europe (Caspers and Freund, 2001; Huijzer and Vandenbergh, 1998; Zagwijn, 1996), and in the north-eastern part of the Netherlands (Van Gijssel, 1995). The paleo-surface temperature proposed by Luijendijk et al. (2011) uses fixed temperatures at fixed time periods. Helmens (2014) and Moreno et al. (2014) give a more accurate and detailed paleo-surface temperature history for Europe. Implementing these alternative paleo-surface

temperature models would not significantly change the modelling results.

4.2. Transient model for paleo-surface temperature

The paleo-surface temperature variations are used as input in a transient thermal 3D model with spatial vertical grid size of 200 m and horizontal grid size of 1 km, taking thermal properties from the high-resolution model of Békési et al. (2020). The transient temperature equation is solved using an explicit 3-step Runge-Kutta finite difference approach with conductive heat transfer (Bonté et al., 2012; Verwer, 1977):

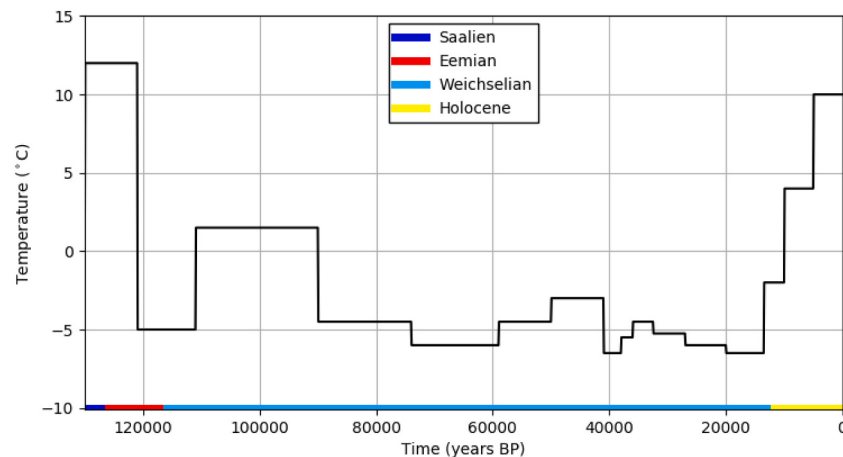


Fig. 6. Paleo-surface temperature history used in the modelling workflow after Luijendijk et al. (2011). Based on published climate proxy data (Caspers and Freund, 2001; Huijzer and Vandenbergh, 1998; Van Gijssel, 1995; Zagwijn, 1996).

$$\frac{\delta T}{\delta t} = \frac{1}{\rho C_p} [\nabla^* (k \nabla T) + A] \text{ with } \nabla = \left(\frac{\delta}{\delta x}, \frac{\delta}{\delta y}, \frac{\delta}{\delta z} \right)^T \quad (2)$$

Where T = temperature [K], ρ = density [kg m^{-3}], C_p = specific heat [$\text{J K}^{-1} \text{kg}^{-1}$], k = thermal conductivity [$\text{W m}^{-1} \text{K}^{-1}$], A = radiogenic heat production [W m^{-3}] and t = time [s].

The temperature of the transient model is initiated at the start of the evolution with a steady state thermal solution in agreement with the paleo surface temperature at the start of the forward model. During the calculation of the paleo-surface temperature correction only the upper boundary condition of surface temperature varies, all other parameters are kept constant. The exact temperature change of the model due to this paleo-surface temperature variation depends on multiple parameters, including uncertainty in thermal properties, uncertainty in paleo-surface temperature, and the effects of phase changes of freezing and melting water in pores (see Annex A). The sensitivity of the model results to these parameters is discussed in Section 6.

4.3. Pseudo-radiogenic heat production for paleo-surface temperature effects in the 3D steady state model

The transient model results in a perturbed geotherm compared to steady state conditions. The transient model for the paleo-surface temperature variations is computationally effective in a single run but would provide a major computational burden for the full high resolution 3D models in the last steps of the workflow with thousands of runs with ES-MDA data-assimilation. For these models, the steady state approximation allows for a 5–10 times faster computational performance, compared to a fully transient approach. In order to mimic the thermal signature of the perturbation by paleo-surface temperature effects in the 3D steady modelling workflow, we translate the observed change in thermal gradient with depth (and underlying variation in heat flow) in the transient model by adopting a correction radiogenic heat production for the steady state model, which can reproduce the same change in thermal gradient in the steady state model. The depth dependent correction for the heat production ΔA in the 3D steady state model is determined as:

$$\Delta A(z_i) = \frac{q(z_i) - q(z_{i-1})}{\Delta Z} - A(z_i) \quad (3)$$

Where z_i is depth of the node i in the 3D grid, $A(z_i)$ is the prior heat production of the model and $q(z_i)$ is heat flow in the 1D transient model at depth z_i which is determined from the thermal gradient and thermal conductivity in the model as:

$$q(z_i) = -k \frac{dT}{dz}(z_i) \quad (4)$$

We set the corrected A in the 3D model as a fixed parameter before the final run with extensive data assimilation. A fixed radiogenic heat production now allows the model to slightly change conductivities and heat flow during the final run of data assimilation, while preserving in a correct way the cooling effect of paleo-surface temperatures. In this way the cooling effect is not overprinted by the final data assimilation.

For calibration of the model during the final modelling workflow step, only temperature measurements of the “Combined database” are used because of the vertical resolution of the 3D model as described in Section 3.1.

4.4. Characteristics of the 3D model

The forward modelling workflow uses a variety of assumptions in terms of subsurface properties. Parameter values are chosen from

lithological interpretation based on Hantschel and Kauerauf (2009) for specific geologic formations (Békési et al., 2020). Since these geologic formations consist of several different lithologies, there is a lot of variance within one geologic formation in terms of thermal properties. Due to three data assimilation steps within the modelling workflow (Békési et al., 2020) the model is able to slightly vary properties within sedimentary units to better represent subsurface properties and mitigate temperature mismatches. Due to computational limitations the vertical resolution of the model is 200 m. Several wells from the “Shallow database” have been individually modelled with a small horizontal grid dimension centred around the borehole location. Because of the small horizontal grid, a 10–20 times higher vertical grid resolution could be used compared to the national model. Investigating the influence of grid resolution showed that vertical grid resolution of 10 m resulted in <0.7 °C deviation from the 200 m resolution model in the top 1000 m.

5. Results

5.1. Reproduction of paleo-surface temperature cooling effect

We compared forward model predictions of the transient model with temperature observations of the shallow database at each well location. At first, we inspected the capability of the model in reproducing the effect of paleo-surface temperatures on the subsurface temperature in a 1D homogeneous model over the past 130,000 years with identical starting conditions and with model assumptions in agreement with Ter Voorde et al. (2014). The model is marked by a steady state geotherm for the top 10 km, with radiogenic heat production of $A = 3.6 \mu\text{W m}^{-3}$, thermal conductivity of $k = 2 \text{ W m}^{-2} \text{ K}^{-1}$. Boundary conditions for the initial steady state temperature are a surface heat flow of $q_s = 66 \text{ mW m}^{-3}$ and surface temperature of $T_s = 12^\circ\text{C}$:

$$T(z) = T_s + \frac{q_s}{k} z - \frac{A}{2k} z^2 \quad (5)$$

Fig. 7 shows the 1D homogeneous transient model for the paleo surface temperature correction (step 6b) as well as the steady state pseudo-radiogenic heat production (step 6c, eq. (3)). Both models reproduce the perturbed present day geotherm from Ter Voorde et al. (2014) well.

The model results show a significant effect on the temperature, with over 10 °C cooling around 1 km depth, whereas at 2–4 km depth the cooling effect gradually disappears. As explained in Section 3, the data examination shows that observed temperatures of the whole onshore Netherlands indicate geotherms between 20 °C km⁻¹ and 25 °C km⁻¹ for the upper few hundred meters, similar to the reduction of the thermal gradient in the top sections of Fig. 7. This observation on national scale is consistent with the fact that paleo-surface temperature effects are geographically expected to be rather uniform on the scale of the Netherlands. The model also highlights the importance of adopting a paleo-surface temperature correction in the 3D modelling workflow in order to reproduce the strong vertical variability in heat flow and associated geothermal gradient.

5.2. Updated 3D subsurface temperature model

Fig. 8 shows the modelled temperatures of the updated 3D subsurface temperature model with a similar colour scale as Fig. 4. Implementation of paleo-surface temperatures in the 3D modelling workflow results in cooler modelled temperatures to a depth of ~2500 m. Therefore, the updated 3D subsurface temperature model better matches temperatures for observations from the “Shallow database” (Fig. 9) and “Deep database” (Fig. 10). Differences between the model with and

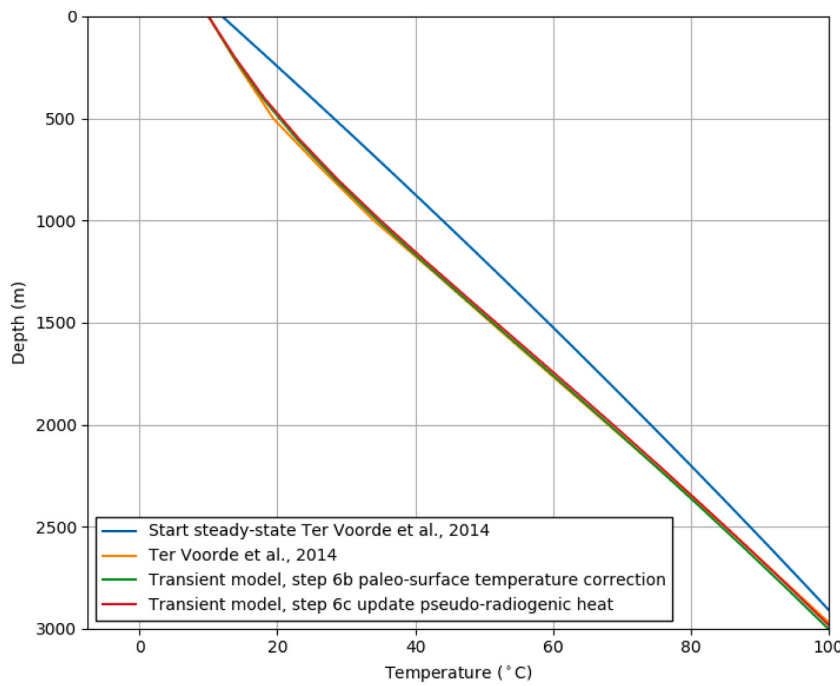


Fig. 7. Geotherms in the upper 3 km for the steady state starting condition, present day 1D homogeneous temperature model and from Ter Voorde et al. (2014).

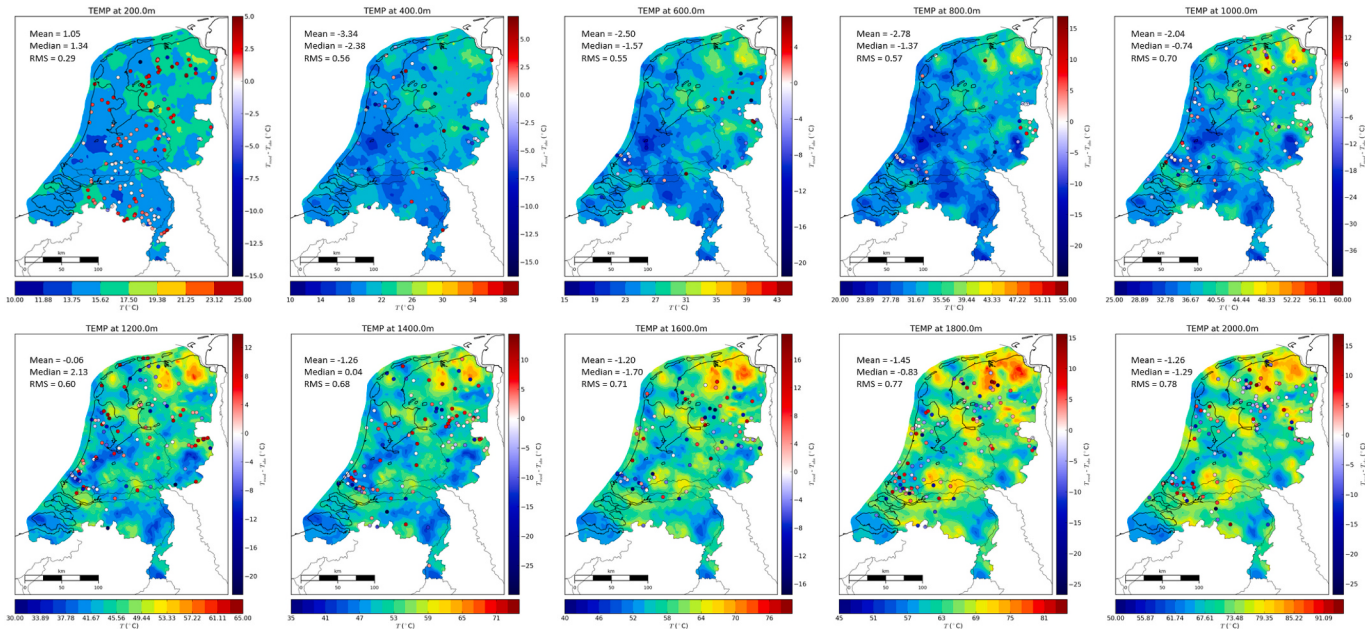


Fig. 8. Isodepth temperature maps of the onshore Netherlands between 200 and 2000 m depth of the updated 3D subsurface temperature model. Modelled temperatures minus observed temperatures from the “Combined database” are plotted on top with circles within a ± 100 m interval. Note the different colour scale for modelled temperatures at various depth. “Mean”, “Median” and “Root Mean Square (RMS)” values refer to the difference between the modelled temperature and the data.

without paleo-surface temperature correction are at maximum up to 10 °C at ~ 1 km depth (Fig. 10). Fig. 4 (previous model) and Fig. 8 (updated 3D subsurface thermal model) display mean, median and root mean square (RMS) values for every isodepth map, which are consistently better for the updated 3D subsurface temperature model. Only RMS values at 1600, 1800 and 2000 m depth are slightly better in previous model of Békési et al. (2020), while mean and median values at the same depth are significantly improved in case of the updated 3D subsurface temperature model. Where the previous model

overestimated 74% of the temperature observations of the “Combined database” down to a depth of 2 km, the updated 3D subsurface temperature model only overestimates 48% of the observations, of which 81% of the overestimated temperatures originates from the “Shallow database” and 45% from the “Deep database”. In the 2–6 km domain, there is barely any difference between the two models (Fig. 11, $>\sim$ rank 800), with 53% versus 54% underestimated temperatures in the previous and updated 3D subsurface temperature model respectively.

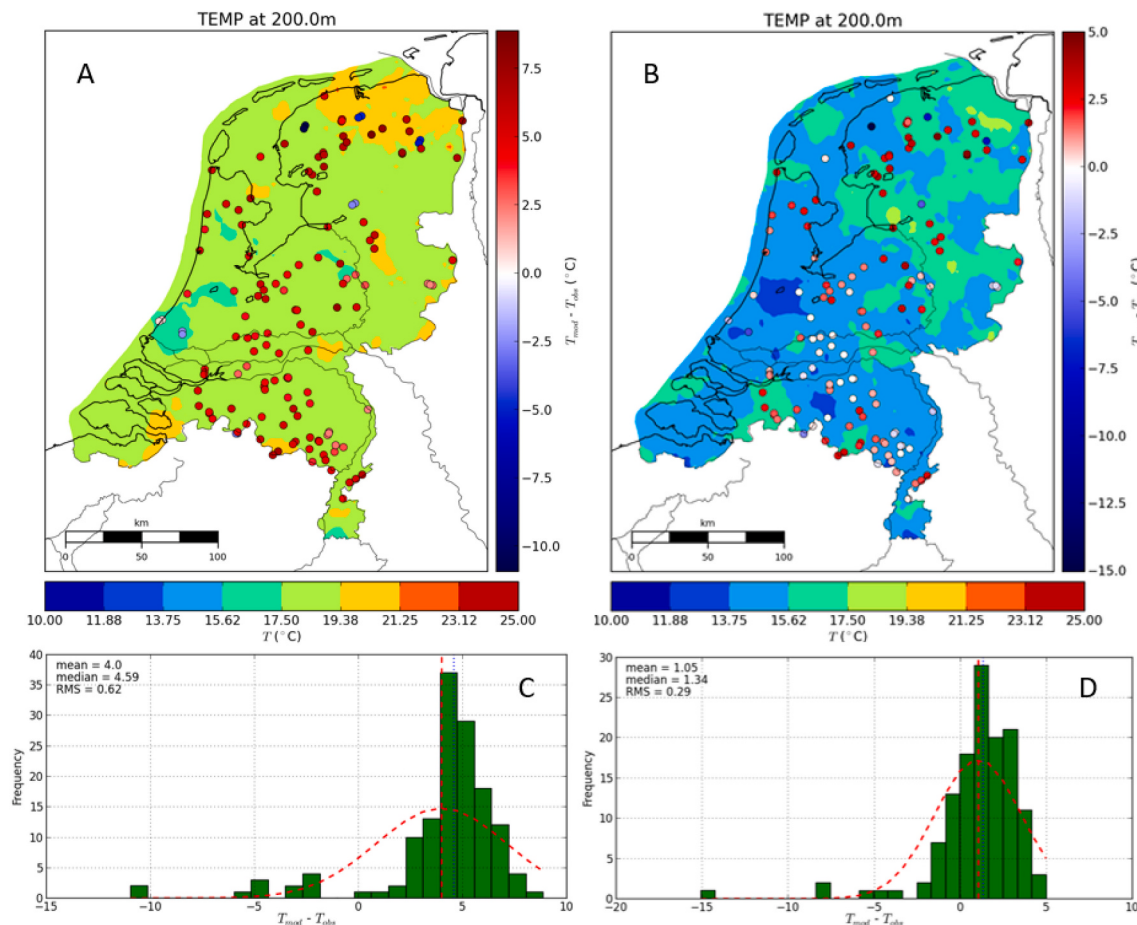


Fig. 9. Isodepth maps of previous model (Békési et al., 2020) (a) versus updated 3D subsurface thermal model (b) at 200 m depth showing a difference between the two models up to ~5 °C. Beneath are the corresponding histograms showing the occurrence of difference between the previous model (c) and updated 3D subsurface thermal model (d) versus measured temperature at 200 ± 100 m depth, including the mean, median and RMS values of the models.

6. Sensitivity analysis

In this section, the sensitivity of the predicted temperature correction upon individual parameters is analysed. For the adopted paleo-surface temperature history, there is an uncertainty in the adopted temperatures, as well as the exact moment of change in surface temperature. The changes in surface temperature used in this model are abruptly and not gradual (Fig. 6). The used paleo-surface temperature history is therefore not an exact reconstruction of the actual paleo-surface temperature. For this reason, we investigated the influence of possible variation in paleo-temperature history and the control of thermal properties in the thermal response.

Monitoring the evolution of the geotherm within the 1D homogeneous temperature model shows that small paleo-surface temperature changes between 90,000 and 13,500 yr. BP have no effect on the present day geotherm. The entire Weichselian glaciation is basically the reason of the colder subsurface temperatures observed, which results in an almost linear geotherm at the end of the Weichselian period (Fig. 12). The paleo-surface temperature history of the Holocene, following the Weichselian glaciations, determines the amount of heating in the upper part of the subsurface down to 1000 m depth. Evidently, the sharp increase in paleo-surface temperature during the Holocene effectively

heated the top part of the present-day geothermal gradient but was not able to influence temperatures at depths exceeding 1500 m (Fig. 12). Because of the strong influence of Holocene paleo-surface temperatures, a better estimation of the paleo-surface temperature history for this time period could possibly improve modelling results. Luijendijk et al. (2011) and Ter Voorde et al. (2014) showed that paleo-surface temperatures during the considered time interval of 130,000 years still influence the present day geotherm at deeper levels up to 3–4 km depth.

The values for conductivity (k), specific heat (C_p) and density (ρ) and radiogenic heat production (A) have been adopted from previous studies (Békési et al., 2020). The first three parameters determine the thermal diffusivity (α) of the subsurface at a certain location and depth:

$$\alpha = \frac{k}{\rho C_p} \quad (6)$$

We varied the thermal diffusivity by 10% to inspect the sensitivity of the results. As a consequence, the effects of paleo-surface temperatures variations penetrate deeper or shallower into the subsurface. This effect is best visible without the final step of extensive data assimilation and is shown in Fig. 13. There is hardly any effect at the top section up to ~1500 m depth, however some degrees difference is visible at larger depth. Since there is almost no change in modelled temperatures

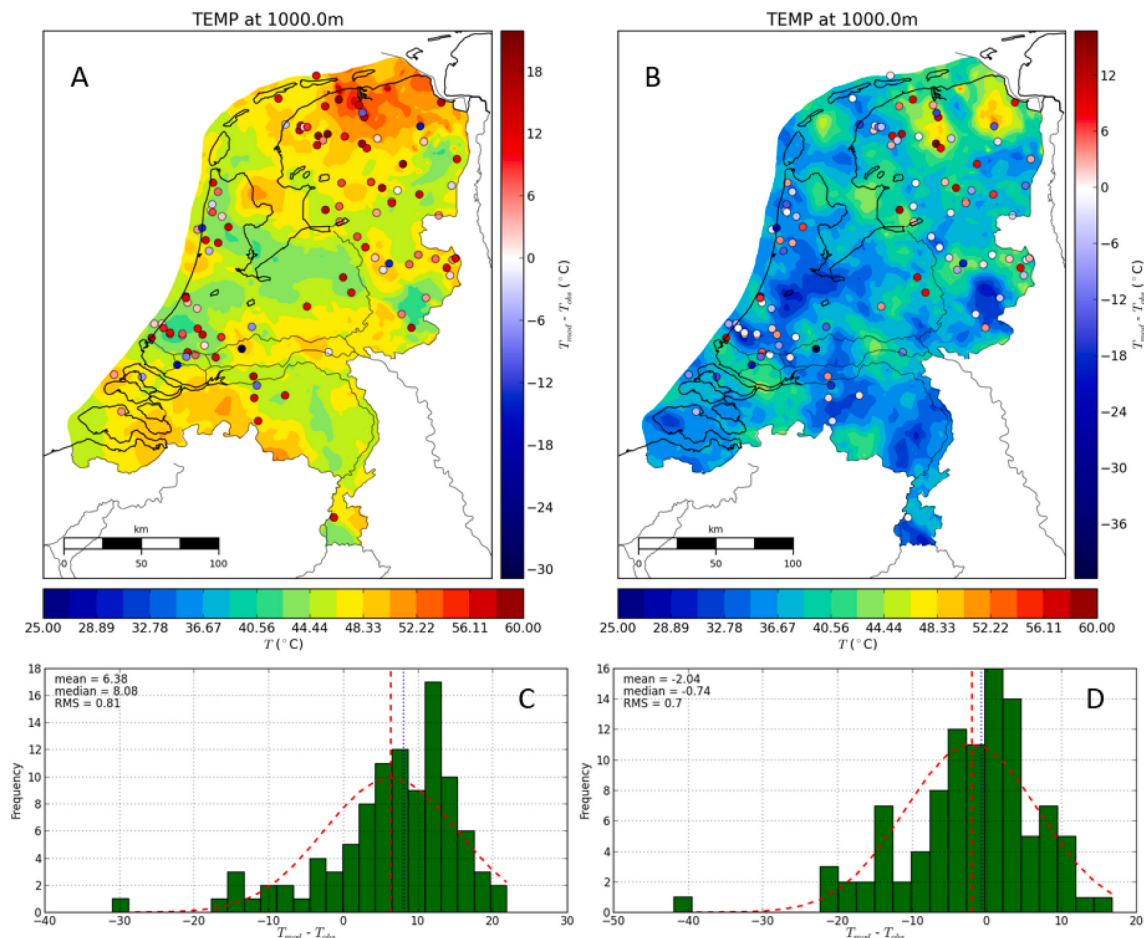


Fig. 10. Isodepth maps of previous model (Békési et al., 2020) (a) versus updated 3D subsurface thermal model (b) at 1 km depth showing a difference between the two models up to 10°C . Beneath are the corresponding histograms showing the occurrence of difference between the previous model (c) and updated 3D subsurface thermal model (d) versus measured temperature at 1000 ± 100 m depth, including the mean, median and RMS values of the models.

between previous (Békési et al., 2020) and updated 3D subsurface temperature model in the 2–6 km interval (Fig. 11), the sensitivity of the model as a consequence of thermal diffusivity is limited, because it is overprinted by the final data assimilation.

7. Discussion

The influence of latent heat related to phase changes of water in porous space in the model was tested. Paleo-surface temperatures created permafrost paleo-conditions in the upper part of the subsurface with temperatures down to -6.5°C . This means that energy is used during the chosen paleo-surface temperature history to freeze or melt water in porous space of subsurface rocks which potentially decreases the depth penetration of the effect of varying paleo-surface temperature (Ter Voorde et al., 2014). In the model the effect of latent heat for freezing and melting has been incorporated as described in annex A. The effect at present day of this additional correction for latent heat did not exceed 0.02°C . Investigating the influence of latent heat over time in more detail shows that there are more significant paleo-differences for the top 400 m between models excluding and including a latent heat correction. The maximum difference for the top 400 m is in the order of 1.0°C . These findings agree with previous studies (e.g. Šafanda et al.,

2004), showing that phase change effects on temperature are of importance at locations that have undergone more recent permafrost conditions than the Netherlands.

The shallow temperature distribution may also be influenced by sedimentation, erosion and crustal deformation. The modelling assumed that during the past 130,000 yr. these processes did not have a major effect. Within this time interval, most sedimentation occurred during the Eemian and Upper Pleistocene. Starting at the Saalian-Eemian boundary, sedimentation rates of less than 0.5 mm yr^{-1} on average can be found in the Amsterdam region, which is relatively high for this period in the Netherlands (Cleveringa, 1998; Gibbard, 2003). For the Roer Valley Graben a sedimentation rate of only 0.05 mm yr^{-1} was calculated (Houtgast et al., 2002). It is unlikely that such low sedimentation rates create major differences in terms of temperature, in agreement with earlier findings of Van Wees et al. (2009) and Bonté et al. (2012). Thereafter, these processes have not been investigated in more detail.

Relatively large anomalies in modelled and observed temperatures in the 0–500 m depth interval are all related to data in the “Deep database” and can be attributed to somewhat lower quality data (Fig. 2b). However, anomalies found at shallow depth originating from the “Shallow database” are likely to be caused by groundwater (convective) flow, either related to salt diapirs or to concentrated areas of infiltration

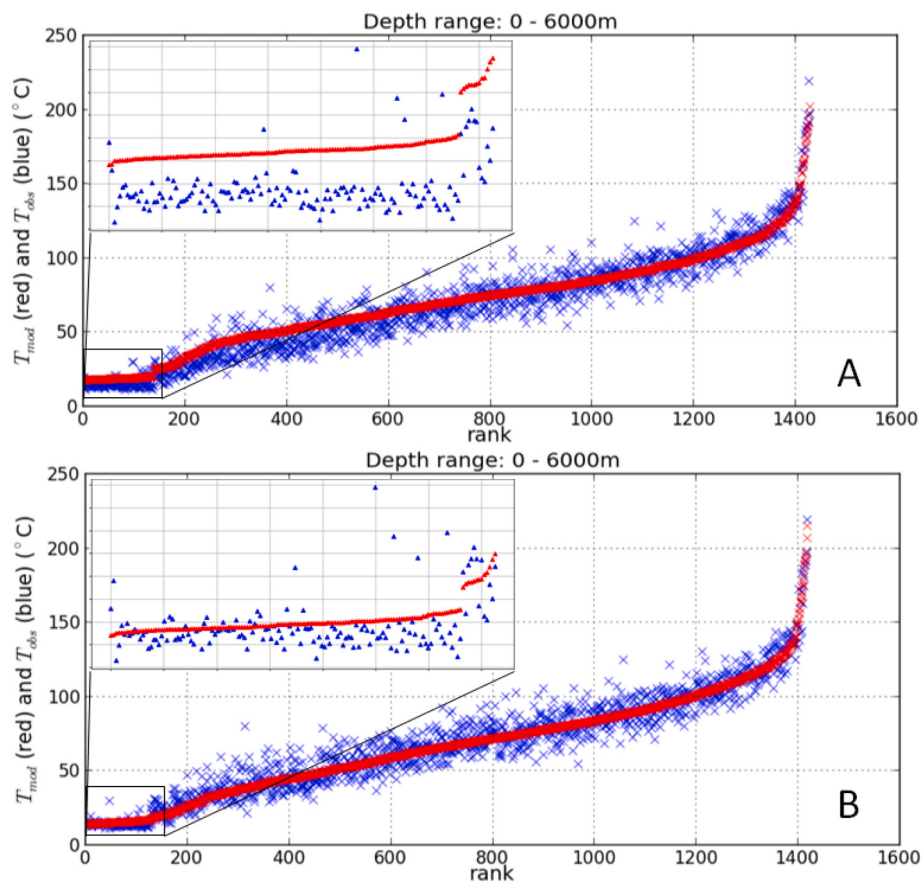


Fig. 11. Plot showing model estimations (red) compared to observations (blue, all data is $<15^{\circ}\text{C}$ accurate) for previous model (a) of Békési et al. (2020) and updated 3D subsurface temperature model (b) with the modelled temperatures ranked on the x-axis. (For interpretation of the references to colour in this figure legend, the reader is referred to the web version of this article.)

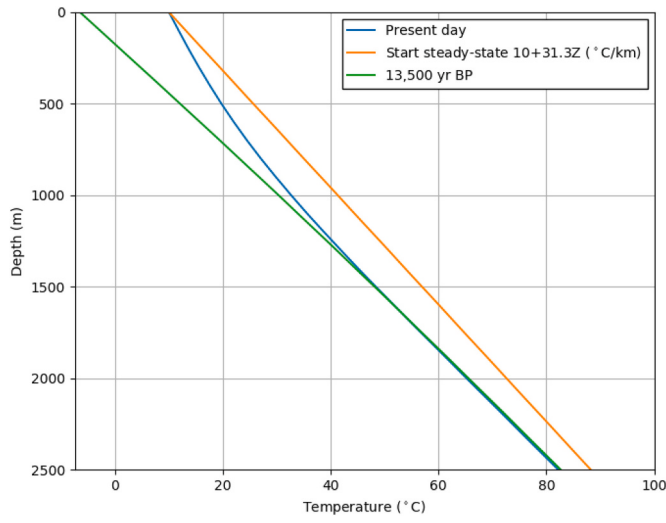


Fig. 12. Geothermal gradient of the start (steady state), 1D homogeneous temperature model before the beginning of the Holocene at 13500 yr. BP and the present day geotherm of the 1D homogeneous temperature model.

(Smith and Chapman, 1983; Kooi, 2016; Bense et al., 2020). Luijendijk et al. (2011) and Van Balen et al. (2002) stated that local thermal anomalies can be linked to deep infiltration of water into fault zones. Zechstein salt acts as an impermeable layer that influences deep

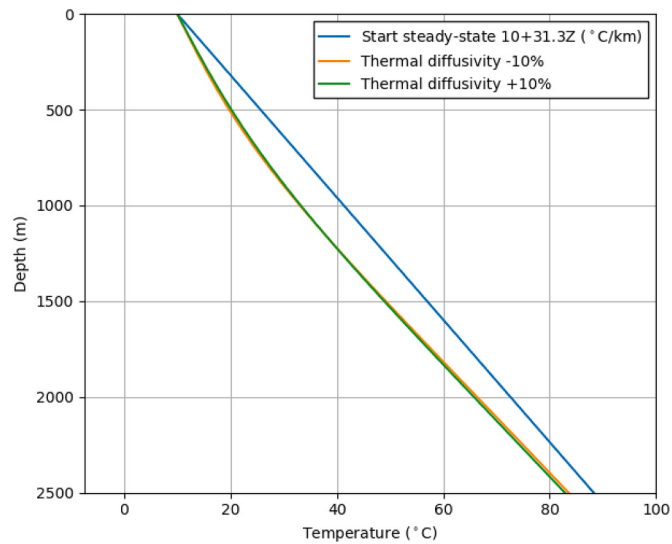


Fig. 13. Modelled geothermal gradients at present day after implementing the same paleo-surface temperature history for an 1D homogeneous model versus the steady state starting condition with a 10% thermal diffusivity increase or decrease.

groundwater flow directions and can facilitate convective groundwater flow (Elshehawi et al., 2019). Zechstein salt is more abundant in the North-East of the Netherlands and strongly varies in thickness due to diapirism up to several hundred meters below the surface (Verweij,

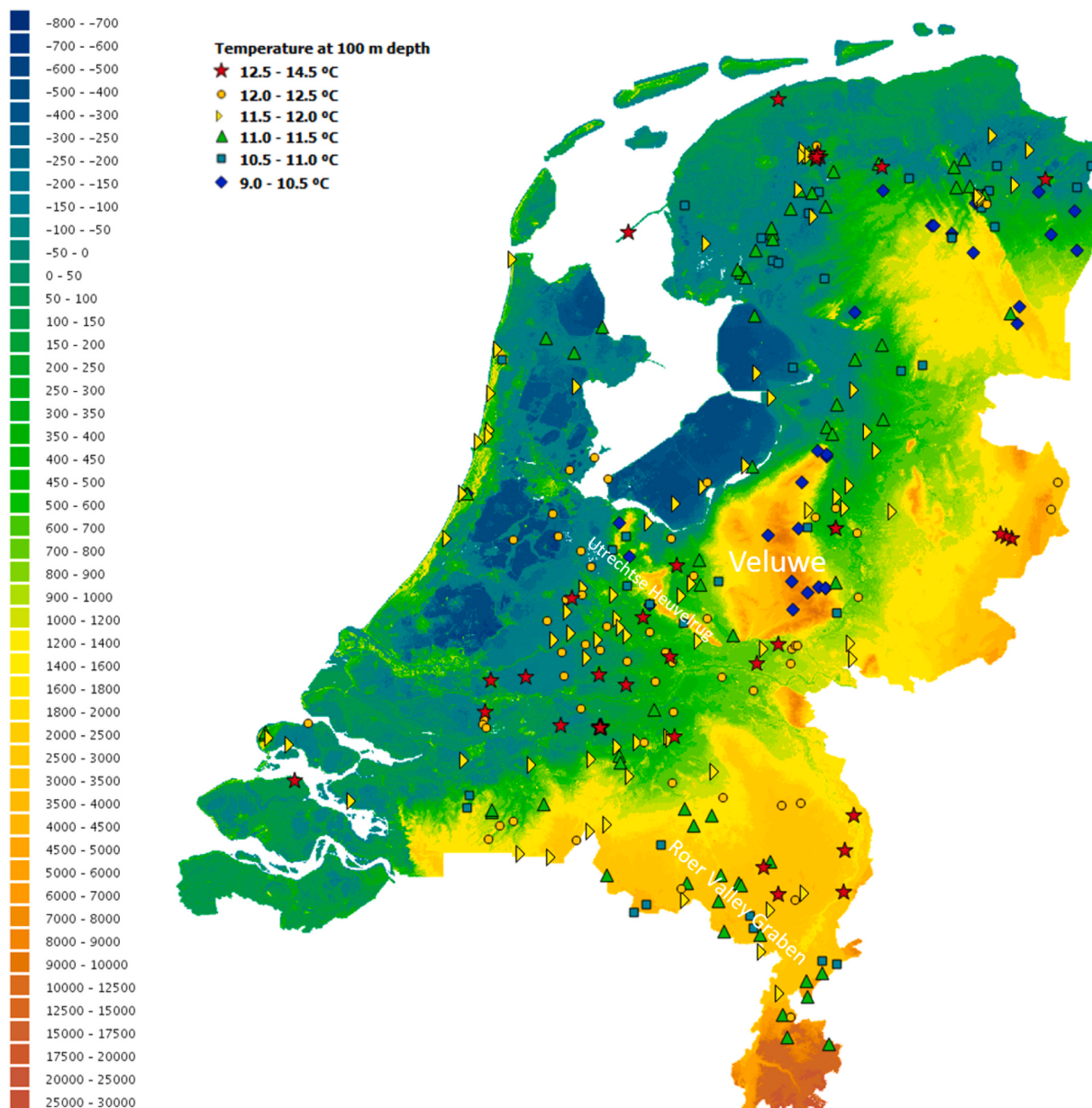


Fig. 14. Observation temperatures of the Netherlands at 100 m depth (0.1 °C accurate), plotted on top of an altitude relative to NAP (cm) map of the Netherlands from www.ahn.nl. Indicated in white the locations of the “Veluwe”, “Utrechtse Heuvelrug” and “Roer Valley Graben” respectively.

2003). The effects of deep groundwater flow on temperature distribution can be very capricious with major differences over small distances. The large distance between datapoints is unlikely to be able to capture temperature anomalies created due to deep groundwater flow. A more detailed layering of the shallow subsurface, employing more detailed available subsurface models and forward simulation of groundwater flow, could improve the modelled temperature field.

In addition, infiltration areas like “the Veluwe” and “the Utrechtse Heuvelrug” and fault plane related flow patterns like the “Roer Valley Graben” can explain thermal anomalies (Luijendijk et al., 2011) (Fig. 14). The first two areas, both moraines, are distinguishable from

surrounding areas not only by elevated altitudes but also by depleted temperatures down to depths of 200 m according to the “Shallow database”. The third area is a major fault system in the Netherlands, located in the southern Netherlands with a NW-SE strike. This fault system is recognizable in the temperature data by decreased temperatures in the graben and higher temperatures at the horst side of the fault (Fig. 14). Strong vertical flow of fluids along the fault plane is likely to cause this temperature anomaly in southern the Netherlands (Luijendijk et al., 2011). These examples indicate that there is a strong link between shallow groundwater convection flow patterns and minor temperature anomalies observed. Modelling these temperature anomalies requires

the implementation of a subsurface convection flow model into the 3D modelling workflow. Since the modelling workflow is suitable to model these minor temperature anomalies by slightly varying conductivities of subsurface layers during data assimilation, implementing a subsurface convection flow model is not likely to create major improvements of the model.

The inferred widespread cooling of the shallow subsurface, has implications for the potential of shallow geothermal systems within the Netherlands. Decreased temperatures at shallow depth relative to the previous models indicate that geothermal systems and HT-ATES sites need to be downgraded in terms of effectiveness. The updated 3D subsurface temperature model therefore has a negative effect on profitable geothermal development in the Netherlands for the top ~1500 m of the subsurface. However, these new results provide more trust in geothermal potential estimates as the models are higher quality. The extended modelling workflow including a paleo-surface temperature correction which can be effectively adopted in steady state thermal workflows is relevant not only for the Netherlands but worldwide applicable. The effect of paleo-surface temperatures on present-day subsurface temperatures depends on the specific regional location and corresponding varying regional thermal properties. Including the effect of latent heat would dampen the influence of glacial periods but has an effect of less than 0.02 °C on the present day thermal field in the Netherlands, which is expected to be bigger in areas with more recent permafrost conditions (Šafanda et al., 2004).

8. Conclusion

We presented a novel workflow which is well capable to incorporate paleo-surface temperature effects in steady state 3D conductive temperature models. The workflow builds from approximating the transient effects, using appropriate source and sink terms for radiogenic heat production in the steady state model. This allows for rapid models, which can be easily used in ensemble approaches for data assimilation of

high-resolution temperature models for geothermal resource assessment.

The relevance of the model has been demonstrated by an updated 3D subsurface temperature model of the onshore Netherlands. For data constraints, we combined an extensive subsurface temperature database with more than 1500 deep (1–6 km) temperature measurements combined with over 200,000 shallow (<600 m) temperature measurements to be used for calibration. This combined temperature database represents two separate geothermal gradients; a shallow geothermal gradient of ~20 °C km⁻¹ for the top 400 m underlain with a deep geothermal gradient of ~31 °C km⁻¹ for the 2–4 km interval.

Previous 3D subsurface temperature models systematically overpredict temperatures at shallow (<2000 m) depth, whereas our updated model successfully removes bias towards overprediction of temperatures in the shallow subsurface. The regular distribution of overpredicted temperatures in previous models demonstrates the uniform influence of paleo-surface temperatures over large areas. Incorporating the glaciation effect of the Weichselian glacial period and subsequent Holocene temperature rise turned out to be the missing link between the two distinct geothermal gradients. This explains the systematically overpredicted temperatures at shallow (<2000 m) depth within previous models. Furthermore, the updated 3D subsurface temperature model shows that the paleo-surface temperature effect is hardly overprinted by groundwater flow.

The updated model, marked by up to 10 degrees cooling compared to models ignoring the paleo-surface temperature effects, has major implications for assessing geothermal resource potential down to 2 km depth.

Declaration of Competing Interest

The authors declare that they have no known competing financial interests or personal relationships that could have appeared to influence the work reported in this paper.

Appendix A Annex: latent heat for melting and freezing

During the Weichselian glaciation a permafrost front penetrated the Dutch subsurface to depths exceeding 200 m (Govaerts et al., 2015). In the numerical solution melting and freezing is implemented by a modification of the heat capacity at the phase transition (0 °C). Because only water in the porous space can freeze or melt, the porosity of the subsurface rocks determines the amount of water in the rock. It is assumed that all porous space in subsurface rocks is filled with water. For the modelling of the effect of including latent heat, a relatively high porosity $\Theta = 0.4$ is used for all rocks, since the phase transition affects only the shallow subsurface.

The latent heat of freezing/melting of water L_0 [333,600 J kg⁻¹] (Mottaghy and Rath, 2006) is added to the specific heat capacity of water at the freezing temperature. The latent heat is adopted into the finite difference formulation (eq. (2)) by a temperature dependent volumetric heat capacity $\rho C_p(T)$:

$$\rho C_p(T) = (1 - \Theta)\rho_m C_{p_m} + \Theta\rho_f(C_{p_f} + L(T)) \quad (\text{A1})$$

Where T is temperature and $\rho C_p(T)$ is determined as a volume average over the matrix (subscript m) and fluid/ice fraction (subscript f), and includes the latent heat by the term L(T). L(T) is represented by a Gaussian function in order to distribute the latent heat over a temperature range close to the freezing point:

$$L(T) = \frac{L_0}{C\sqrt{2\pi}} \exp\left(-\frac{(T - B)^2}{2C^2}\right) \quad (\text{A2})$$

B represents the freezing point of 0 °C and C is set to 0.5 °C. The distribution over a small temperature interval is required for the correct solution of the finite difference formulation and has been adopted in other studies (Mottaghy and Rath, 2006) (Fig. A1). The densities have been chosen $\rho_m = 2700 \text{ kg m}^{-3}$, $\rho_f = 1000 \text{ kg m}^{-3}$ and heat capacities $C_{p_m} = 1000 \text{ J kg}^{-1} \text{ K}^{-1}$, $C_{p_f} = 4180 \text{ J kg}^{-1} \text{ K}^{-1}$. Other thermal properties have been adopted from Békési et al. (2020) and Ter Voorde et al. (2014) as explained in the main text.

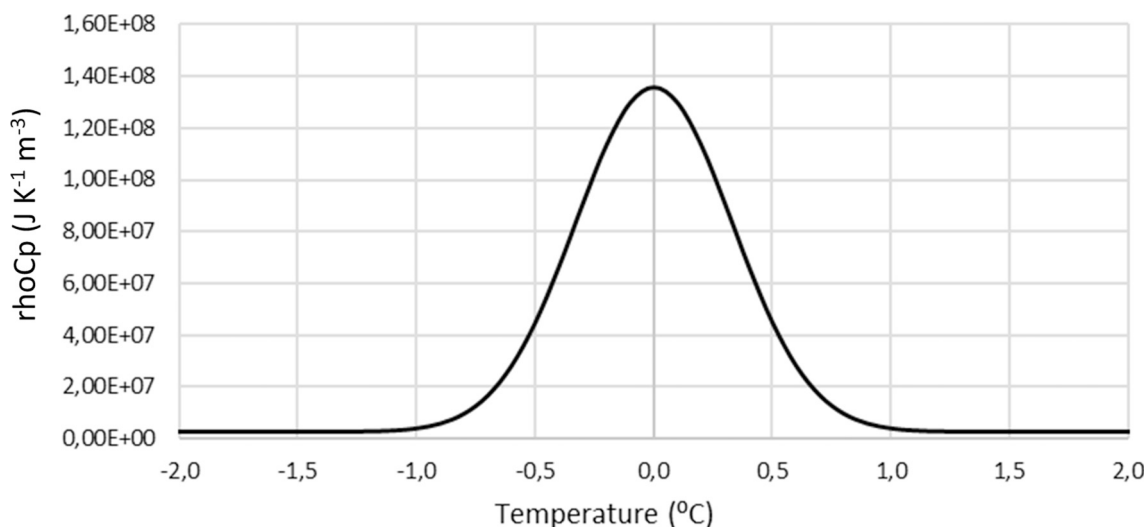


Fig. A1. $\rho C_p(T)$ in the vicinity of the freezing temperature of 0 °C.

The model does not take into account fluctuations in yearly temperatures and ignores seasonal variations in the surface temperature conditions. Temperatures may however vary every year and even within seasons. Therefore, melting and freezing, especially close to the surface would occur more frequent than assumed in our model. The purpose of this correction is to see effects on depths exceeding changes in seasonal or yearly fluctuations. This means that for calculating the thermal field at depths of over ~100 m the used timesteps and freezing interval are suited. Differences in physical properties of ice compared to water have been neglected in our approach. The density, specific heat and conductivity of ice differ from fluid water. Furthermore, for the chosen temperature interval where phase transition takes place, a partition function could determine the percentage of ice to fluid (Mottaghy and Rath, 2006).

Including the effect of latent heat would dampen the influence of glacial periods but has an effect of less than 0.02 °C on the present-day thermal field in the Netherlands.

References

- Beardmore, G.R., Rybach, L., Blackwell, D., Baron, C., 2010. A protocol for estimating and mapping global EGS potential. *Geoth. Res. T.* 34, 301–312.
- Békési, E., Struijk, M., Bonté, D., Veldkamp, H., Limberger, J., Fokker, P.A., Vrijlandt, M., van Wees, J.D., 2020. An updated geothermal model of the Dutch subsurface based on inversion of temperature data. *Geothermics* 88, 101880.
- Bense, V.F., Kooi, H., 2004. Temporal and spatial variations of shallow subsurface temperature as a record of lateral variations in groundwater flow. *Journal of Geophysical Research: Solid Earth* 109 (B4).
- Bense, V.F., Kurylyk, B.L., de Bruin, J.G.H., Visser, P., 2020. Repeated subsurface thermal profiling to reveal temporal variability in deep groundwater flow conditions. *Water Resources Research* 56 (6), e2019WR026913.
- Bodri, L., Čermák, V., 2011. *Borehole Climatology: A New Method how to Reconstruct Climate*. Elsevier.
- Bonté, D., Van Wees, J.D., Verweij, J.M., 2012. Subsurface temperature of the onshore Netherlands: new temperature dataset and modelling. *Neth. J. Geosci.* 91 (4), 491–515.
- Buik, N., Stolk, P., Willemsen, G., 2004. Analyse van temperatuurmetingen in de Nederlandse ondergrond. *Stromingen* 10 (4), 13–22.
- Carlson, T., 2019. Petrophysical Report of the Dinantian Carbonates in the Dutch Subsurface. <https://www.nlog.nl/scan>.
- Caspers, G., Freund, H., 2001. Vegetation and climate in the Early-and Pleni-Weichselian in northern Central Europe. *Journal of Quaternary Science* 16 (1), 31–48.
- Cleveringa, P., 1998. Borehole Amsterdam-Terminal: Pollen Analytical Data of the Eemian Type Area. Volume of Abstracts: The Eemian, p. 15.
- Cloetingh, S., Van Wees, J.D., Ziegler, P., Lenkey, L., Beekman, F., Tesar, M., Förster, A., Norden, B., Kabán, M., Hardebol, N., 2010. Lithosphere tectonics and thermo-mechanical properties: an integrated modelling approach for enhanced Geothermal Systems exploration in Europe. *Earth. Rev.* 102 (3–4), 159–206.
- Conrads, L.A., 1975. Observations of Meteorological Urban Effects: The Heat Island of Utrecht. Doctoral dissertation. Rijksuniversiteit Utrecht.
- De Jager, J., 2003. Inverted basins in the Netherlands, similarities and differences. *Neth. J. Geosci.* 82 (4), 339–349.
- Elshehawi, S., Bregman, E., Schot, P., Grootjans, A., 2019. Natural isotopes and ion compositions identify changes in groundwater flows affecting wetland vegetation in the Drentsche Aa Brook Valley, the Netherlands. *Journal of Ecological Engineering* 20 (3).
- Emerick, A.A., Reynolds, A.C., 2013. Ensemble smoother with multiple data assimilation. *Comput. Geosci.* 55, 3–15.
- Gibbard, P.L., 2003. Definition of the Middle–Upper Pleistocene boundary. *Glob. Planet. Chang.* 36 (3), 201–208.
- Gola, G., Bertini, G., Bonini, M., Botteghi, S., Brogi, A., De Franco, R., Manzella, A., 2017. Data integration and conceptual modelling of the Larderello geothermal area, Italy. *Energy Procedia* 125, 300–309.
- Hantschel, T., Kauerauf, A.I., 2009. *Fundamentals of Basin and Petroleum Systems Modeling*. Springer Science & Business Media.
- Helmens, K.F., 2014. The Last Interglacial–Glacial cycle (MIS 5–2) re-examined based on long proxy records from central and northern Europe. *Quat. Sci. Rev.* 86, 115–143.
- Houtgast, R.F., Van Balen, R.T., Bouwer, L.M., Brand, G.B.M., Brijker, J.M., 2002. Late Quaternary activity of the Feldbiss Fault Zone, Roer Valley Rift System, the Netherlands, based on displaced fluvial terrace fragments. *Tectonophysics* 352 (3–4), 295–315.
- Huang, S.P., Pollack, H.N., Shen, P.Y., 2008. A late Quaternary climate reconstruction based on borehole heat flux data, borehole temperature data, and the instrumental record. *Geophys. Res. Lett.* 35 (13).
- Huijzer, B., Vandenberghe, J., 1998. Climatic reconstruction of the Weichselian Pleniglacial in northwestern and Central Europe. *Journal of Quaternary Science* 13 (5), 391–417.
- Kappelmeyer, O., Haenel, R., 1974. *Geothermics with Special Reference to Application*. In: Berlin Gebrüder Borntraeger Geoexploration Monographs Series, 4.
- Kombrink, H., Van Lochem, H., Van Der Zwan, K.J., 2010. Seismic interpretation of Dinantian carbonate platforms in the Netherlands; implications for the palaeogeographical and structural development of the Northwest European Carboniferous Basin. *J. Geol. Soc.* 167 (1), 99–108.
- Kombrink, H., Doornenbal, J.C., Duin, E.J.T., Den Dulk, M., Ten Veen, J.H., Witmans, N., 2012. New insights into the geological structure of the Netherlands; results of a detailed mapping project. *Neth. J. Geosci.* 91 (4), 419–446.
- Kooi, H., 2008. Spatial variability in subsurface warming over the last three decades; insight from repeated borehole temperature measurements in the Netherlands. *Earth Planet. Sci. Lett.* 270 (1–2), 86–94.
- Kooi, H., 2016. Groundwater flow as a cooling agent of the continental lithosphere. *Nat. Geosci.* 9 (3), 227–230.
- Kukkonen, I.T., Rath, V., Kivekäs, L., Šafanda, J., Čermák, V., 2011. Geothermal studies of the Outokumpu Deep Drill Hole, Finland: Vertical variation in heat flow and palaeoclimatic implications. *Phys. Earth Planet. Inter.* 188 (1–2), 9–25.
- Limberger, J., Calcagno, P., Manzella, A., Trumpy, E., Boxem, T., Pluymakers, M., van Wees, J.D., 2014. Assessing the prospective resource base for enhanced geothermal systems in Europe. *Geothermal Energy Science* 2 (1), 55–71.
- Limberger, J., Boxem, T., Pluymakers, M., Bruhn, D., Manzella, A., Calcagno, P., van Wees, J.D., 2018. Geothermal energy in deep aquifers: A global assessment of the resource base for direct heat utilization. *Renewable and Sustainable Energy Reviews* 82, 961–975.

- Lipsey, L., Pluymakers, M., Goldberg, T., van Oversteeg, K., Ghazaryan, L., Cloetingh, S., van Wees, J.D., 2016. Numerical modelling of thermal convection in the Luttegeest carbonate platform, the Netherlands. *Geothermics* 64, 135–151.
- Luijendijk, E., Ter Voorde, M., Van Balen, R., Verweij, H., Simmelink, E., 2011. Thermal state of the Roer Valley Graben, part of the European cenozoic rift system. *Basin Res.* 23 (1), 65–82.
- Majorowicz, J., Šafanda, J., Torun-1 Working Group, 2008. Heat flow variation with depth in Poland: evidence from equilibrium temperature logs in 2.9-km-deep well Torun-1. *Int. J. Earth Sci.* 97 (2), 307–315.
- Majorowicz, J., Wybraniec, S., 2011. New terrestrial heat flow map of Europe after regional paleoclimatic correction application. *Int. J. Earth Sci.* 100 (4), 881–887.
- Moreno, A., Svensson, A., Brooks, S.J., Connor, S., Engels, S., Fletcher, W., Genty, D., Heiri, O., Labuhn, I., Persiou, A., Peyron, O., Sadori, L., Valero-Garcés, B., Wulf, S., Zanchetta, G., 2014. A compilation of Western European terrestrial records 60–8 ka BP: towards an understanding of latitudinal climatic gradients. *Quat. Sci. Rev.* 106, 167–185.
- Peters, J., van Dalsen, W., Steinmetz, J., 1983. Temperatuurmetingen bruikbaar bij onderzoek naar verbreiding van infiltratiewater uit persputten KIWA. *Groundwater Survey TNO* (unpublished TNO report).
- Pollack, H.N., Huang, S., 2000. Climate reconstruction from subsurface temperatures. *Annu. Rev. Earth Planet. Sci.* 28 (1), 339–365.
- Šafanda, J., Szewczyk, J., Majorowicz, J., 2004. Geothermal evidence of very low glacial temperatures on a rim of the Fennoscandian ice sheet. *Geophys. Res. Lett.* 31 (7).
- Sissingh, W., 2004. Palaeozoic and Mesozoic igneous activity in the Netherlands: a tectonomagmatic review. *Neth. J. Geosci.* 83 (2), 113–134.
- Smit, J., van Wees, J.D., Cloetingh, S., 2018. Early Carboniferous extension in East Avalonia: 350 my record of lithospheric memory. *Mar. Pet. Geol.* 92, 1010–1027.
- Smith, L., Chapman, D.S., 1983. On the thermal effects of groundwater flow: 1. Regional scale systems. *Journal of Geophysical Research: Solid Earth* 88 (B1), 593–608.
- Stolk, P., 2000. Analyse van temperatuurmetingen in de nederlandse ondergrond (20–300 m beneden maaiveld) in relatie tot hydrologische en meteorologische omstandigheden in heden en verleden. IF Technology/Vrije Universiteit (unpublished IF report).
- Ter Voorde, M., Van Balen, R., Luijendijk, E., Kooi, H., 2014. Weichselian and Holocene climate history reflected in temperatures in the upper crust of the Netherlands. *Neth. J. Geosci.* 93 (3), 107–117.
- Unger, J., 1992. The Seasonal System of Urban Temperature Surplus in Szeged. *Acta Climatologica*.
- Van Adrichem Boogaert, H., Kouwe, W., 1993. Stratigraphic nomenclature of the Netherlands, revision and update by RGD and NOGEPA. *Med. Rijks Geol. Dienst.* 50.
- Van Balen, R.T., Verweij, J.M., Van Wees, J.D., Simmelink, H., Van Bergen, F., Pagnier, H., 2002. Deep subsurface temperatures in the Roer Valley Graben and the Peelblock, the Netherlands-new results. *Neth. J. Geosci.* 81 (1), 19–26.
- Van Dalsen, W., 1980a. The shallow subsurface temperature field in the Netherlands. In: *Advances in European Geothermal Research*, pp. 496–505.
- Van Dalsen, W., 1980b. Temperatuuronderzoek waterwingebied de groeve. *Groundwater Survey TNO* (unpublished TNO report).
- Van Dalsen, W., 1981a. Temperatuuronderzoek 1980 vuilstort noordwijk. *Groundwater Survey TNO* (unpublished TNO report).
- Van Dalsen, W., 1981b. Geothermal Investigations in Shallow Observation Wells. *Groundwater Survey TNO* (unpublished TNO report).
- Van Dalsen, W., 1983a. Temperatuuronderzoek bij de kunstmatige grondwateraanvulling onder de winplaats haren. *Groundwater Survey TNO* (unpublished TNO report).
- Van Dalsen, W., 1983b. Het Ondiep Ondergrondse Temperatuurveld in Nederland. *Groundwater Survey TNO* (unpublished TNO report).
- Van Dalsen, W., 1998. Inventarisatie van geologische en geofysische gegevens van een gebied om de waterwinplaats genderen. *Groundwater Survey TNO* (unpublished TNO report).
- Van Gijsel, K., 1995. A hydrogeological and palaeoenvironmental data set for large-scale groundwater flow model simulations in the northeastern Netherlands. *Meded. Rijks Geol. Dienst* 52, 105–134.
- Van Hulten, F.F.N., Poty, E., 2008. Geological factors controlling Early Carboniferous carbonate platform development in the Netherlands. *Geol. J.* 43 (2–3), 175–196.
- Van Wees, J.D., Stephenson, R.A., Ziegler, P.A., Bayer, U., McCann, T., Dadlez, R., Gaupp, R., Narkiewicz, M., Bitzer, F., Scheck, M., 2000. On the origin of the southern Permian Basin, Central Europe. *Mar. Pet. Geol.* 17 (1), 43–59.
- Van Wees, J.D., Van Bergen, F., David, P., Nepveu, M., Beekman, F., Cloetingh, S.A.P.L., Bonté, D., 2009. Probabilistic tectonic heat flow modeling for basin maturation: Assessment method and applications. *Mar. Pet. Geol.* 26 (4), 536–551.
- Van Wees, J.D., Kronimus, A., Van Putten, M., Pluymakers, M.P.D., Mijnlieff, H., Van Hooff, P., Obdam, A., Kramers, L., 2012. Geothermal aquifer performance assessment for direct heat production—Methodology and application to Rotliegend aquifers. *Neth. J. Geosci.* 91 (4), 651–665.
- Verweij, J.M., 2003. Fluid Flow Systems Analysis on Geological Time Scale in Onshore and Offshore Netherlands.
- Verwer, J.G., 1977. A class of stabilized three-step Runge-Kutta methods for the numerical integration of parabolic equations. *J. Comput. Appl. Math.* 3 (3), 155–166.
- Wesselink, M., Liu, W., Koornneef, J., van den Broek, M., 2018. Conceptual market potential framework of high temperature aquifer thermal energy storage—a case study in the Netherlands. *Energy* 147, 477–489.
- Zagwijn, W.H., 1996. An analysis of Eemian climate in western and Central Europe. *Quat. Sci. Rev.* 15 (5–6), 451–469.
- Zhu, K., 2013b. Urban Heat Island in the Subsurface and Geothermal Potential in Urban Areas (Doctoral Dissertation, Ph. D. thesis, Eberhard Karls Universität Tübingen).

References only used in the appendix

- Govaerts, J., Beerten, K., Ten Veen, J., 2015. Numerical simulation of Permafrost Depth in the Netherlands. In: Appendix 1 of Report OPERA-PU-TNO412, vol. 44.
- Mottaghy, D., Rath, V., 2006. Latent heat effects in subsurface heat transport modelling and their impact on palaeotemperature reconstructions. *Geophysical Journal International* 164 (1), 236–245.